Soft Matter

PAPER

View Article Online
View Journal

Cite this: DOI: 10.1039/c9sm00727j

Propagating density spikes in light-powered motility-ratchets

Celia Lozano, †[a] Benno Liebchen, †*[bc] Borge ten Hagen,†[bd] Clemens Bechinger [a] and Hartmut Löwen [b]

Received 10th April 2019,
Accepted 17th May 2019

DOI: 10.1039/c9sm00727j

rsc.li/soft-matter-journal

Combining experiments and computer simulations, we use a spatially periodic and flashing light-field to direct the motion of phototactic active colloids. Here, the colloids self-organize into a density spike pattern, which resembles a shock wave and propagates over long distances, almost without dispersing. The underlying mechanism involves a synchronization of the colloids with the light-field, so that particles see the same intensity gradient each time the light-pattern is switched on, but no gradient in between (for example). This creates pulsating transport whose strength and direction can be controlled *via* the flashing protocol and the self-propulsion speed of the colloids. Our results might be useful for drug delivery applications and can be used to segregate active colloids by their speed.

1 Introduction

Active colloids are autonomously navigating microparticles that consume energy while moving. They comprise living microorganisms like bacteria, algae and sperm,[1–3] but also man-made synthetic swimmers, which can be produced with desired properties. Such synthetic microswimmers are often based on anisotropic colloidal Janus particles that are self-propelled by phoretic mechanisms either directly induced by catalytic surfaces evoking chemical reactions,[4,5] or initiated by light[6–12] or other external fields, such as ultrasonic,[13] magnetic[14–17] or electric[18,19] ones.

While free active colloids show diffusive random motion on large scales,[20,21] equivalent to the motion of passive colloids at high temperature, applications to use them *e.g.* for targeted drug delivery[22,23] or nanorobotics[24] require to direct and steer their motion on demand.

One way to direct the motion of active particles is to expose them to a periodic but asymmetric potential landscape (ratchet), leading to directed transport,[25–28] in a way similar to passive colloids driven out of equilibrium through additional time-dependent fields.[29–31] Characteristically, such potential ratchets involve forces acting on the center of mass coordinate of the particles, yielding a spatial variation of their potential energy. A versatile alternative to create directed transport in active colloids is so-called motility-ratchets, which specifically exploit the active nature of the particles and have no direct counterpart for passive colloids. These ratchets hinge on the spatial modulation of the self-propulsion speed (or direction) through an external field,[27,32,33] not affecting the potential energy of the particles. Here, the required modulation of the self-propulsion speed can be achieved *e.g.* for light-sensitive Janus colloids in a suitable standing light-wave,[32] which has been previously discussed in the context of dynamical trapping of active particles in the dark spots of the light-field.[34,35] An interesting extension of such static motility-ratchets, providing an additional handle to control the active particle dynamics, is to use a time-dependent motility field, as recently considered theoretically,[36–38] and also experimentally[39] for light-sensitive bacteria.[40–42]

In the present work, we combine simulations and experiments to establish a flashing motility-ratchet for synthetic phototactic colloids, based on a sawtooth-shaped light-pattern with intensity $I(x,t)$ which we periodically switch on and off (flashing). The gradients of I create an effective torque affecting the colloids' self-propulsion direction, which can systematically bias their motion,[32,43] yielding directed transport. Here, the emergence of transport hinges on a phototactic torque biasing the active particles' direction of motion, as opposed to classical flashing potential ratchets,[30,44] usually depending on the interplay of time-dependent forces and diffusion. This novelty in the working mechanism of the flashing motility-ratchet manifests in a set of remarkable features. In particular, we find that the individual active particles synchronize with the flashing light-field and self-organize into density-spikes resembling a coherently moving shock-wave. As their most striking feature, these spikes hardly disperse, opposing the usual situation

[a] *Fachbereich Physik, Universität Konstanz, 78457 Konstanz, Germany*
[b] *Institut für Theoretische Physik II: Weiche Materie, Heinrich-Heine-Universität Düsseldorf, 40225 Düsseldorf, Germany*
[c] *Institut für Festkörperphysik, Technische Universität Darmstadt, 64289 Darmstadt, Germany. E-mail: liebchen@fkp.tu-darmstadt.de*
[d] *Physics of Fluids Group and Max Planck Center Twente, Department of Science and Technology, MESA+ Institute, and J. M. Burgers Centre for Fluid Dynamics, University of Twente, 7500 AE Enschede, The Netherlands*
† These authors contributed equally.

in potential ratchets, where the interplay of time-dependent forces and diffusion leads to strong dispersion of any localized particle ensemble. Thus, the present setup opens a route to use laser-light to create pulsating transport allowing one to 'bombard' a distant target with short and intense pulses of active particles, as might be interesting, in particular, for drug-delivery applications. Here, the transport velocity can be systematically controlled *via* the flashing times, but interestingly, it also depends sensitively on the particle speed in the off-phase. In particular, we find that the transport direction even reverts when changing the self-propulsion speed of the particles in the off-phase. This transport reversal can be used, in principle, to segregate ensembles of fast and slow particles and might serve as a useful tool for the preparation of clean ensembles of active particle with near identical self-propulsion speed.

Before detailing these findings, let us sketch the physical mechanism underlying the flashing motility-ratchet: if the torque acting on the active colloids scales linearly with the gradient of the laser field (unsaturated regime) no transport can occur in static light-patterns. (This contrasts[32] with operating in the saturated regime.) Intuitively, if noise is negligible, this is because the phototactic torque acting on particles crossing a whole spatial period first turns them in a certain direction and then back to the original orientation, so that a localized and unbiased initial ensemble remains unbiased for all times. Flashing in turn allows the particles to synchronize with the light-field in such a way that they repeatedly see the same gradient when the light-pattern is on and a uniform field in each off-phase, provoking persistent unidirectional motion. This dynamics is based on a limit cycle attractor in the underlying phase space, which represents a late-time dynamics where particles move by exactly one spatial period per flashing cycle, in suitable parameter regimes. Since all particles which are attracted by the same limit cycle show one and the same periodic dynamics at late times they move coherently with a speed dictated by the limit-cycle, leading to almost dispersion-free transport – a key feature of the present work.

2 Model

For conceptual clarity, we first introduce an idealized flashing motility ratchet, based on an effective phototactic torque which scales linearly with the light gradient ($\omega \propto |\nabla I|$). In this case, the emerging transport is flashing-induced and vanishes in static light-patterns. To see this, consider self-propelled Janus particles, actively moving in 2D with a self-propulsion speed $v(x,t)$, varying both in space and time, as controlled by the imposed light-field (see Fig. 1). For simplicity, we specifically consider a quasi 1D modulation of the light-field, and hence of v. The self-propulsion direction $\hat{\mathbf{u}} = (\cos\phi, \sin\phi)$ changes in response to an effective phototactic torque, and also due to rotational diffusion, yielding:

$$\dot{\mathbf{r}} = v(x,t)\hat{\mathbf{u}} + \sqrt{2D_t}\boldsymbol{\zeta}_{\mathbf{r}}(t), \quad (1)$$

$$\dot{\phi} = \omega(x,\phi,t) + \sqrt{2D_r}\zeta_{\phi}(t). \quad (2)$$

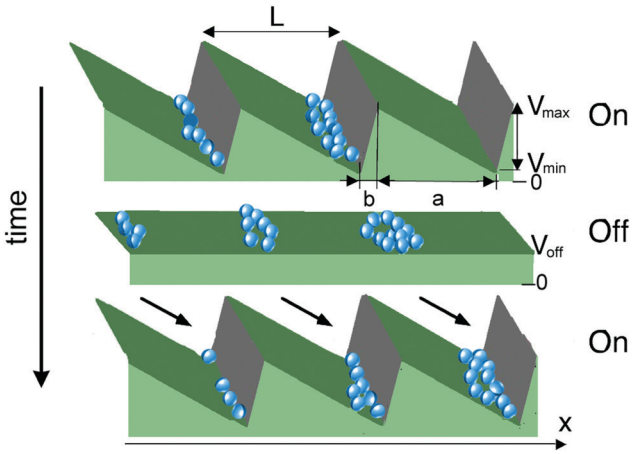

Fig. 1 Schematic: active colloids polarize and self-organize into density spikes propagating resonantly through the flashing light-field. Here, the colloids synchronize with the flashing light-field and a macroscopic fraction of them essentially follow the same periodic trajectory, as dictated by a limit cycle of the system, so that particles within each density spike move coherently. This creates pulsating particle transport with low dispersion. The shown sawtooth-shaped profile represents the particle's self-propulsion velocity, which varies between v_{min} and v_{max} when the light-pattern is on ("on-phase"), where a and b determine the steepness of the gradient, and which everywhere equals v_{off} when the light-field is uniform (middle panel, "off-phase").

Here $\mathbf{r} = (x,y)$ and D_t, D_r are translational and rotational diffusion coefficients; $\boldsymbol{\zeta}_{\mathbf{r}}(t)$ and $\zeta_{\phi}(t)$ represent Gaussian white noise of zero mean and unit variance. The key-quantity controlling the particle dynamics in the light-field is the phototactic alignment rate ω, which reads

$$\omega(x,\phi,t) = Av(x,t)v'(x,t)\sin\phi \quad (3)$$

where $v'(x,t) = \partial v(x,t)/\partial x$. Eqn (3) presents a linear relationship between the alignment rate and the intensity gradient, $\omega \propto |\nabla I|$, which is realistic for shallow light-patterns,[32] but will later be generalized towards saturation effects. Here, the coefficient A follows from experiments.[32] For the velocity profile $v(x,t)$, we choose a sawtooth-shape in the on-phase, as sketched in Fig. 1, with segment lengths a and b and minimal and maximal velocities of v_{min} and v_{max} respectively. In the off-phase the velocity is uniform $v(x,t) = v_{off}$.

Note that in general, besides creating an effective torque aligning the particles, light gradients also induce effective forces creating particle translations, represented by a term $\propto \nabla I$ on the r.h.s. of eqn (1). In accordance with ref. 32, we here neglect such a term for simplicity, but emphasize its existence for future reference.

3 Flashing-induced coherent transport

Let us now explore the dynamics of a representative particle ensemble in the flashing light-field (Fig. 1). We choose random initial positions and orientations uniformly distributed within one unit cell of the sawtooth-shaped light-pattern ($x \in [0,L)$ and $\phi \in [0,2\pi)$) and define the average transport velocity as

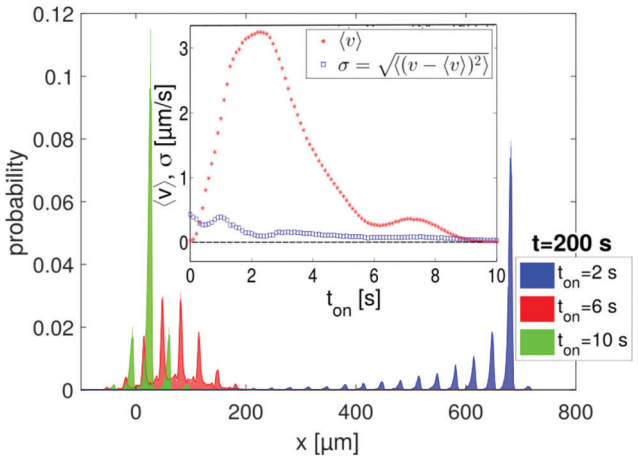

Fig. 2 Propagating density spikes: spatial particle distribution after t = 200 s for N_p = 50 000 and different t_{on} shown in the key. Inset: Mean transport velocity $\langle v\rangle$ and standard deviation $\sigma = \sqrt{\langle (v-\langle v\rangle)^2\rangle}$ as a function of t_{on}, calculated for N_p = 100 and $t_{end} = 30T$ per data point. The dashed line shows the zero line to guide the eye. Parameters: $t_{on} + t_{off}$ = 10 s; a = 27.38 μm; b = 6.02 μm; v_{min} = 3 μm s^{-1}; v_{max} = 13 μm s^{-1} and v_{off} = 3 μm s^{-1}; $A \approx 0.65$ s μm^{-1} ($A = C_1C_2/R$ for particles with radius R = 1.365 μm and C_1 = 0.44 and C_2 = 2.01 s being experimentally determined parameters, see ref. 32).

$\langle v\rangle = \lim_{t\to t_{end}} [x(t) - x(0)]/t$, where t_{end} is some time, large enough that $\langle v\rangle$ is basically stationary (in practice, we additionally average $\langle v\rangle$ over N_p initial conditions). Now performing Brownian dynamics simulations (see footnote ‡ for details) until $t = t_{end}$ for various t_{on} but a fixed flashing period $T = t_{on} + t_{off}$, we generically find directed transport for all values of t_{on} (Fig. 2, inset). In contrast, however, for the static cases $t_{on} = 0$ and $t_{off} = T$ (uniform light-field) and $t_{on} = T$ and $t_{off} = 0$ (static sawtooth-shaped light-pattern) the transport vanishes. That is the directed transport is flashing-induced.

Before exploring the origin and properties of the flashing-induced transport, let us first understand its absence in uniform light-fields. To see this, note that particles crossing a whole spatial period of a static light-pattern (t_{on} = 10 s) do not experience any net alignment, which can be seen as follows for the noise-free case: from eqn (1)–(3) and $\dot{\phi} = \dot{x}(\partial\phi/\partial x)$, it follows that for vanishing noise we have $\partial\phi/\partial x = Av'(x)\tan\phi(x)$, which yields after integration over a spatial period $\phi(x + L) = \phi(x)$. Thus, in the absence of noise, if all particles are initialized with uniformely distributed orientations in an intensity-maximum of the light-field, exactly half of them permanently move to the left and to the right respectively, *i.e.* there is no transport. (For spatially distributed initial ensembles, we provide a slightly more general argument for the absence of transport in footnote 45.) Our argument for the absence of transport breaks down in the presence of flashing. Intuitively, flashing allows the particles to synchronize with the light-field in such a way that they "see" the same gradient each time the light-field is switched on and no gradient when the light-field is off. This repeatedly aligns their self-propulsion in the same direction, as we further detail in Section 4.

The synchronization of the particle motion with the light-field has a number of remarkable consequences. One of them is shown in Fig. 2 (inset), where we can see that the standard deviation $\sigma = \sqrt{\langle v^2\rangle - \langle v\rangle^2} \ll \langle v\rangle$, for most values of t_{on}. That is, the transported particle ensemble hardly disperses, but moves rather coherently through the flashing light-field. In particular, σ has a minimum at $t_{on} \approx 2.6$ s where the transport velocity is maximal. To further illuminate the particle dynamics in the flashing motility-ratchet, let us consider the spatial particle distribution in the light-pattern, a snapshot of which after 20 driving cycles is shown in Fig. 2. As we can see in this figure, for t_{on} = 10 s, where we have no transport, most particles are localized around their initial positions; they collectively move back and forth in the light-pattern. Conversely, for t_{on} = 2 s the particle distribution is strongly asymmetric and shows a train of pronounced peaks resembling a shock wave. This train persistently moves to the right, with a speed of precisely one spatial period per flashing cycle ($\langle v\rangle = L/T$).

Apart from exploring the dependence of the transport velocity on the parameters of the environment, such as the flashing duration t_{on}, it is instructive to also explore the dependence of the transport velocity on the particle properties: in Fig. 3, we show the transport velocity as a function of v_{off} (the self-propulsion speed in the off state), finding a remarkable structure, comprising distinct peaks in the transport velocity, and in particular a transport-reversal for 10 μm s$^{-1} \lesssim v_{off} \lesssim$ 20 μm s^{-1}. (Note here that the structure of the peaks is statistically well converged, as indicated by the fact that the standard deviation σ is much smaller than $\langle v\rangle$ for most data points.) Following the observed transport reversal, when considering a mixture of particles with different velocities, say 5 μm s^{-1} and 15 μm s^{-1}, the flashing

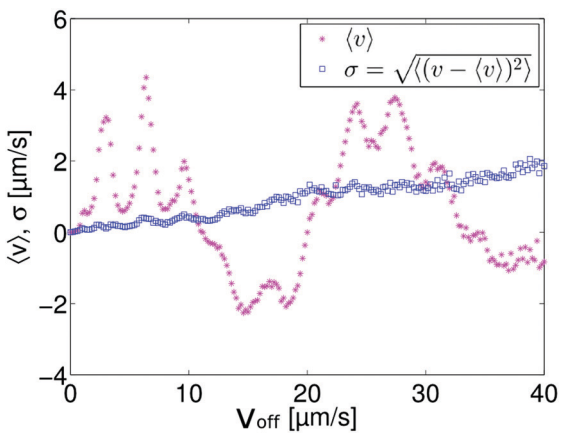

Fig. 3 Transport reversal: mean velocity $\langle v\rangle$ and standard deviation $\sigma = \sqrt{\langle (v-\langle v\rangle)^2\rangle}$ for t_{on} = 2 s as a function of v_{off}. Other parameters as in Fig. 2.

‡ Brownian dynamics simulations have been performed using a standard forward Euler algorithm with a time step of $dt = 0.001T$. Each point in the curves showing averages is based on N_p = 100 trajectories (initial conditions) integrated for $30T$ and distributions are based on N_p = 50 000 initial conditions. The system size is infinite, *i.e.* the simulations do not require any boundary conditions.

light-field will transport them in opposite directions and segregate the mixture. This could be used in principle as a tool to prepare clean ensembles of active particles with a uniform self-propulsion speed. Notice that the presence of a current reversal alone, which is naturally present in many potential ratchets,[29] is not sufficient to achieve clean and near-complete segregation of two initially distributed particle species. Instead, such a segregation requires $|\langle v\rangle| \gtrsim \sigma$ for each species, a condition which is naturally fulfilled for the flashing motility-ratchet (Fig. 3). This shows once more that the intrinsically low dispersion of the emerging transport might be useful for practical applications. Notice, however, that σ increases roughly linearly with v_{off} (Fig. 3) *i.e.* with the distance particles travel within each off-phase. That is, the particle distribution gets broader as v_{off} increases, allowing for clean segregation 'only' for particles which are not too fast.

4 Mechanism

To understand the mechanism leading to a coherently travelling density spike pattern in detail, it is instructive to first explore typical trajectories in the noise-free case ($D_{\mathrm{r}} = D_{\mathrm{t}} = 0$), as visualized in Fig. 4a for the case $t_{\mathrm{on}} = 2$ s. Here, within one or several driving cycles, the orientation of the particles, which align antiparallel to the light-gradient, converges to a steady value of either $\phi = 0$ (or $\phi = 2\pi n$, n being an integer) or to $\phi = (2n+1)\pi$ (particles typically need about 2–4 s to fully turn[32])

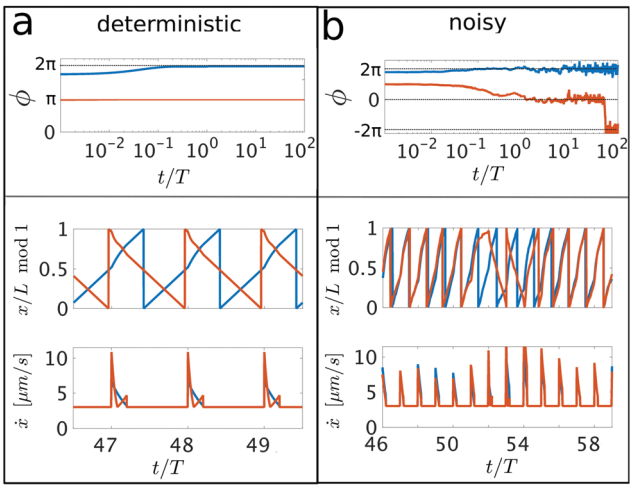

Fig. 4 Transport mechanism in the flashing motility ratchet without (a) and with (b) noise for $t_{\mathrm{on}} = 2$ s and two representative trajectories (blue and orange) with initial orientations $\phi = 3.1$ and $\phi = 5.5$. Without noise, particles fully align with the symmetry axis of the light-field ($\mathbf{p} \times \nabla I = 0$), yielding $\phi = \pi + 2\pi n$ or $\phi = 2\pi n$ ($n \in \mathbb{Z}$), representing motion to the left and to the right, respectively. At late times (middle and lower panel), particles reach a limit cycle attractor and move periodically, with an average speed of exactly $\langle v\rangle = L/T$ (middle panel) either to the left or to the right. In the presence of noise, the particle orientations do not fully converge but fluctuate. Here particles show a dynamics which is similar to the noise-free dynamics most of the time (middle panel), but they can cross-over from one attractor to another one, which can, for example, lead to temporary motion in the opposite direction (middle panel). The shown time intervals have been chosen to representatively illustrate the described dynamics (periodic motion and attractor hopping). Parameters as in Fig. 2.

corresponding to perfect alignment with the axis along which the light-pattern is modulated (upper panel). Once they are aligned, particles no longer experience a torque from the light-field ($\mathbf{p} \times \nabla I(x,t) = 0$ for all x, t) and persistently self-propel in one and the same direction. Conversely to their constant orientation, the speed of the particles still evolves rather irregularly at this stage: it simply reads $\dot{x} = v_{\mathrm{off}}$ in each off-phase, but in the on-phase $\dot{x} \in (v_{\mathrm{min}}, v_{\mathrm{max}})$ it depends on the particle's position at the instance the light-field is switched on. At late times, the dynamics converges to a limit cycle attractor, whose existence is expected from the Poincaré-Bendixon theorem, resulting in a regular, periodic dynamics (Fig. 4a, middle and lower panel). That is particles fully synchronize with the flashing light-field with a temporally periodic speed, whose average is exactly $\langle v\rangle = L/T$ (middle panel), *i.e.* particles propagate by exactly one spatial period L per $T = 10$ s. As illustrated by the blue and the orange curve in Fig. 4a (middle panel), depending on the initial conditions, particles follow a corresponding orbit either to the left or to the right. In this minimal case where only two limit cycles are relevant, each particle propagates with the same one-flashing-cycle-averaged velocity of $\langle v\rangle = L/T$ either to the left or to the right (Fig. 4a, middle and lower panel). The resulting late-time transport velocity is then fully determined by the ratio of initial conditions reaching the limit cycle corresponding to motion to the left and to the right, respectively, *i.e.* to the 'basins of attraction' of the two limit cycles. Specifically for the considered case of $t_{\mathrm{on}} = 2$ s, most of the particles reach an attractor pointing to the right, which generates the transport. (In general, depending on t_{on}, besides limit cycles representing a 1 : 1 resonance, also limit cycles allowing particles to traverse n spatial periods within m driving cycles are allowed, leading to a particle speed of $\langle v\rangle = nL/(mT)$.)

In the presence of noise, ϕ does of course not fully converge to π or 2π but fluctuates even at late times (upper panel in Fig. 4b). However, most of the time (for $t_{\mathrm{on}} = 2$ s) particles still follow a near-resonant dynamics and move with $\langle v\rangle \approx L/T$ (middle panel in Fig. 4b), temporarily resembling trajectories of the underlying deterministic system. Such a dynamics can prolong for many driving cycles. From time to time, however, noise relocates a particle from one limit cycle of the underlying deterministic system to another one, leading, at least temporarily, to a different dynamics. The dynamics shown in Fig. 4b (middle panel) illustrates this: in the time interval between $t \sim 510$ s and $t \sim 550$ s, the orange trajectory crosses from the "$\phi = 0$-attractor" of the underlying noise-free system over to the "$\phi \approx -2\pi$ attractor", yielding the same dynamics, but in between it follows the "$\phi = -\pi$-attractor" for a few flashing cycles and moves in the opposite direction. In the presence of noise, the resulting transport velocity is therefore mainly determined by the time particles spend in the basin of attraction of the limit cycles of the underlying noise-free system. When this basin of attraction is small, as *e.g.* for $t_{\mathrm{on}} = 2$ s for the "$\phi = (2n+1)\pi$-attractor" which leads to motion to the left, particles all move to the right in the long-time average.

The spike pattern observed above now follows quite naturally from the described particle-light-field synchronization. Here, each spike represents a package of particles which have followed

the same limit cycle dynamics for the same amount of time. In particular, particles which have moved for 200 s = 20T with a velocity of $\langle v\rangle \approx L/T = 33.4$ μm/10 s have traversed a distance of $x \approx 20L \approx 668$ μm, which corresponds to the first large peak in Fig. 2 for $t_{on} = 2$ s; the following peaks correspond to particles having traversed a distance of $x \approx 19L$, $18L$, and $17L$, corresponding to particles which have either initially 'lost' time by aligning with a certain delay, or by moving temporarily in the opposite direction. Finally, there is a small peak of particles having traversed a distance $x > 20L$; this corresponds to particles which have been pushed forward during the on-phases before synchronizing with the light-field. (The spike pattern is less clean for $t_{on} = 6$ s and $t_{on} = 10$ s, where the relevant attractors do not correspond to 1 : 1 resonances.)

5 Torque saturation

In experiments the phototactic alignment rate of a Janus colloid with the intensity gradient does not generally increase linearly, as we have assumed so far, but saturates for steep intensity gradients due to thermal coupling.[32] Thus, to compare the flashing motility ratchet with experiments in the next section, we wish to understand the impact of saturation effects first. To this end, we use the following expression for the phototactic alignment rate[32]

$$\omega(x,\phi,t) = v(x,t)\sin\phi\,\mathrm{sgn}(v'(x,t))\frac{C_1}{R}(1-\exp(-C_2|v'(x,t)|)) \quad (4)$$

which approximately reduces to eqn (3) for $|v'(x,t)| \ll 1/C_2$ and $A = C_1C_2/R$ (and exactly for $|v'(x,t)| \to 0$). See Fig. 5 for a comparison of eqn (3) and (4), both in the saturated and in the unsaturated regime. Here, C_2 controls the crossover from the linear to the saturated region. To see the impact of saturation effects, let us now explore the transport velocity as a function of t_{on} (Fig. 6, inset) for $C_2 = 2.01$ s as previously determined in ref. 32. Just as for the unsaturated case (Fig. 2), the transport increases about linearly for small t_{on}, reaches a maximum at $t_{on} \approx 2.6$ s of $\langle v\rangle \gtrsim 3$ μm s^{-1} and then decays again, suggesting that saturation effects have little bearing on the flashing motility ratchet. However, at larger values of t_{on}, the transport plateaus (Fig. 6) rather than decaying towards zero and reaches a finite value of $\langle v\rangle \gtrsim 1.5$ μm s^{-1} for $t_{on} \to 10$ s. That is, saturation effects create directed transport even for a stationary (non-flashing) light-field. This special case has been previously explored in ref. 32. Why do we obtain directed particle

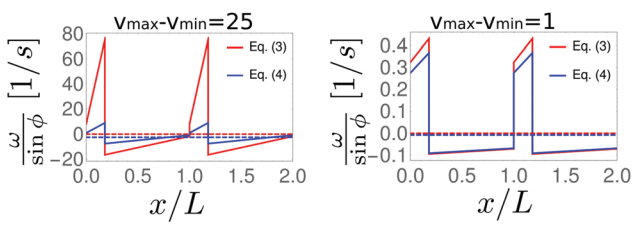

Fig. 5 Red and blue curves represent eqn (3) and (4), respectively, deep in the saturated (left) and in the unsaturated (right) regime. Dashed lines show averages of full curves. Parameters as in Fig. 2.

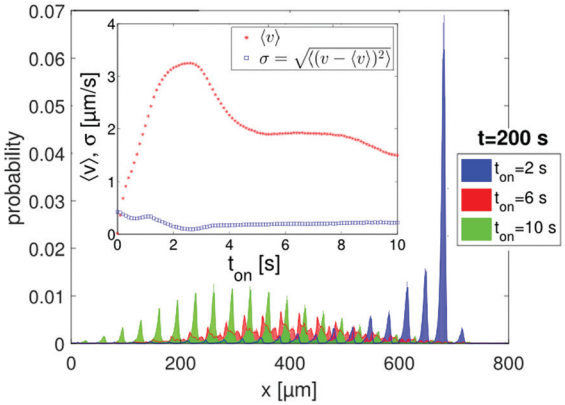

Fig. 6 Impact of torque saturation on the particle distribution and transport velocity. Figures and parameters as Fig. 2 but in the presence of torque saturation, eqn (4) ($C_1 = 0.44$; $R = 1.365$ μm; $C_2 = 2.01$ s, obtained from experiments).

transport here even in the absence of flashing? Note first that the argument for the absence of transport in a static light-pattern as given in Section 3 breaks down in the presence of torque saturation, as $\omega(x,\phi)$ is no longer spatially periodic and a particle crossing a whole spatial period can therefore experience a net change of its orientation (even in the absence of noise).

More constructively, on average, particles need significantly more time to cross the long and shallow a-segments where ∇I is small and the alignment rate is essentially unsaturated (*i.e.* $\omega \propto |\nabla I|$) than for crossing the short and steep b-segments, where ω saturates and is only slightly larger than in the a-segments. Hence, particles leaving a steep b-segment are aligned only weakly as compared to those leaving a a-segment. Thus, particles leaving the b-segment to the left are commonly reflected in the adjacent a-segment, since phototaxis opposes their swimming direction. Conversely, particles leaving an b-segment to the right almost certainly manage to cross the adjacent a-segment where phototaxis is supportive and speeds them up. This breaks the left–right symmetry, initiating transport to the right. (In the extreme case of an almost vertical b-segment and an extremely flat and long a-segment, basically all particles would get reflected when leaving an b-segment to the left, and the ratchet would serve as an "active particle diode".)

To further illuminate the impact of saturation effects, let us explore the particle distribution in the lattice, say after 20 driving cycles. From Fig. 6, we can see that the distribution for $t_{on} = 2$ s is essentially the same as in the absence of saturation effects (Fig. 2), preserving the shock-wave-like profile. As for the transport itself, however, the distribution significantly deviates from the unsaturated case when $t_{on} \sim T$. Following these observations, for our upcoming experiments we expect that saturation effects do not play a strong role if $t_{on} \ll T$. However, if $t_{on} \sim T$, saturation effects are expected to significantly impact the transport.

6 Experiments

To test the flashing motility-ratchet, we now compare our results with experiments. We use light-activated Janus colloids,

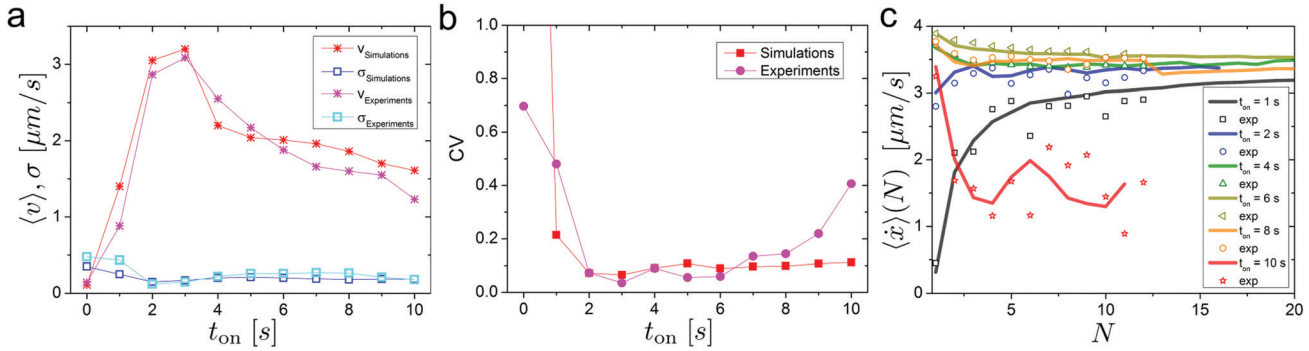

Fig. 7 Comparison of model and experiments: (a) average velocity $\langle v\rangle$ and standard deviation σ, and (b) coefficient of variation (CV = $\langle v\rangle/\sigma$), averaged over the entire simulation/experiment (see text), as a function of t_{on}. Panel (c) shows the average particle velocity in the N-th flashing cycle $\langle \dot{x}\rangle$ for different t_{on} shown in the key. Parameters, both in experiments and simulations, $T_f = t_{on} + t_{off} = 10$ s, $v_{max} = 8\ \mu m\ s^{-1}$, $v_{off} = 4\ \mu m\ s^{-1}$; $v_{min} = 0.8\ \mu m\ s^{-1}$ and $C_1 = 0.44$; $R = 1.365\ \mu m$; $C_2 = 2.01$ s from fits to experiments in ref. 32.

which are composed of optically transparent silica spheres ($R = 1.36\ \mu m$) being capped on one side with 20 nm of carbon. The active colloids are suspended in a critical mixture of water and 2,6-lutidine (lutidine mass fraction 0.286), whose lower critical point is at a temperature of $T_c = 34.1\ ^\circ C$. When the solution is kept at a temperature of $30\ ^\circ C < T_c$, the colloids perform diffusive Brownian motion. Upon laser illumination (at wavelength $\lambda = 532$ nm), where light is absorbed at the caps only, the solvent locally demixes. This creates a concentration gradient accross each colloid's surface, leading to self-propulsion. The resulting self-propulsion speed scales linearly with the laser intensity.[46] The light-pattern, and hence also the motility-pattern, is created by a laser line focus ($\lambda = 532$ nm) being scanned across our sample cell by means of a galvanostatically driven mirror with a frequency of 200 Hz. Synchronization of the scanning motion with the input voltage of an electro-optical modulator leads to a quasi-static illumination landscape. The alternation between a sawtooth-shaped intensity profile and a homogenous one was fully automated using customized software written in LABVIEW. Since the remixing timescale of the binary mixture is on the order of 100 ms,[46] the periodic mirror motion is fast enough to produce stable particle self-propulsion. Particle positions and orientations were obtained by digital video microscopy with a frame rate of 13 fps.

We use a very dilute suspension of microswimmers to avoid particle interactions and subject it to the described flashing ratchet. Here we track the trajectories of particles initialized in one and the same a-segment with uncontrolled initial orientations and let them evolve for $13T$. We repeat the experiment several times and average over $N_p > 25$ trajectories. In Fig. 7a we compare the resulting transport velocity in experiments with our model for various flashing times, finding close quantitative agreement. For the considered parameters, the transport velocity rapidly increases from $\langle v\rangle = 0$ at $t_{on} = 0$ s and approaches a maximal speed of about $\langle v\rangle \gtrsim 3\ \mu m\ s^{-1}$ for $t_{on} \sim 2$–3 s, which is about 2–3 times larger than for the static case. For larger switching times, the transport velocity decreases monotonously with t_{on}. To also compare the dispersion in the model and in the experiments, we show the standard deviation σ also in Fig. 7a, finding near quantitative agreement. It is instructive to visualize this also in a different way. To do this, we define the coefficient of variation as CV = $\langle v\rangle/\sigma$ (quality factor), which is the ratio of the mean transport velocity over the standard deviation, shown in Fig. 7b. While there are notable deviations between experiments and simulations for small and for large t_{on} (Fig. 7b), we find a rather good agreement in the regime $2\ s \leq t_{on} \leq 8$ s, where the transport is dominated by flashing, rather than by torque-saturation effects. This reflects that also in experiments the synchronization between particles and light-field leads to transport with little dispersion. It is instructive to also resolve the time-evolution of the average particle speed in the N-th flashing period, defined as $\langle \dot{x}\rangle(N)$, where the average is taken both over the particle ensemble and the N-th flashing period. Here, both in experiments and in simulations, the transport converges to its steady state value within a few driving cycles in most cases, but takes significantly longer in those cases where dispersion is large ($t_{on} = 1$ s and $t_{on} = 10$ s).

7 Conclusions

Active colloids can synchronize with a sawtooth-shaped flashing light-field and self-organize into a pattern of coherently propagating density spikes. This pattern hardly disperses and yields pulsating particle transport, which might be useful *e.g.* for targeted drug delivery applications. The transport velocity can be tailored by the parameters of the flashing motility field, and remarkably, it reverts when the particle's self-propulsion velocity exceeds a certain threshold. Thus, the present setup can be used as a device for segregating particle ensembles. To observe the latter aspect also in experiments, it would be interesting to do experiments with mixtures of active colloids which are faster than the ones used in the present study, in the future. Our results can be straightforwardly generalized to more complex spatio-temporal motility patterns including random landscapes in space and time, and can be used as a platform to transfer ideas from potential ratchets[29,30,44] to active systems.

Conflicts of interest

There are no conflicts to declare.

Acknowledgements

H. L. and C. B. acknowledge financial support through the priority programme SPP 1726 of the Deutsche Forschungsgemeinschaft (DFG, German Research Foundation). C. B. acknowledges financial support from the ERC Advanced Grant ASCIR (Grant No. 693683). B. t. H. gratefully acknowledges received funding through a Postdoctoral Research Fellowship from the Deutsche Forschungsgemeinschaft – HA 8020/1-1.

References

1 P. Romanczuk, M. Bär, W. Ebeling, B. Lindner and L. Schimansky-Geier, *Eur. Phys. J.-Spec. Top.*, 2012, **202**, 1.
2 J. Elgeti, R. G. Winkler and G. Gompper, *Rep. Prog. Phys.*, 2015, **78**, 056601.
3 M. E. Cates, *Rep. Prog. Phys.*, 2012, **75**, 042601.
4 W. F. Paxton, K. C. Kistler, C. C. Olmeda, A. Sen, S. K. St. Angelo, Y. Cao, T. E. Mallouk, P. E. Lammert and V. H. Crespi, *J. Am. Chem. Soc.*, 2004, **126**, 13424.
5 J. Palacci, C. Cottin-Bizonne, C. Ybert and L. Bocquet, *Phys. Rev. Lett.*, 2010, **105**, 088304.
6 G. Volpe, I. Buttinoni, D. Vogt, H.-J. Kümmerer and C. Bechinger, *Soft Matter*, 2011, **7**, 8810.
7 I. Buttinoni, G. Volpe, F. Kümmel, G. Volpe and C. Bechinger, *J. Phys.: Condens. Matter*, 2012, **24**, 284129.
8 J. Palacci, S. Sacanna, A. Vatchinsky, P. M. Chaikin and D. J. Pine, *J. Am. Chem. Soc.*, 2013, **135**, 15978.
9 J. Palacci, S. Sacanna, A. Preska Steinberg, D. J. Pine and P. M. Chaikin, *Science*, 2013, **339**, 936.
10 J. Palacci, S. Sacanna, S.-H. Kim, G.-R. Yi, D. J. Pine and P. M. Chaikin, *Philos. Trans. R. Soc., A*, 2014, **372**, 20130372.
11 H. Moyses, J. Palacci, S. Sacanna and D. G. Grier, *Soft Matter*, 2016, **12**, 6357.
12 F. Schmidt, B. Liebchen, H. Löwen and G. Volpe, *J. Phys. Chem.*, 2019, **150**, 094905.
13 W. Wang, L. A. Castro, M. Hoyos and T. E. Mallouk, *ACS Nano*, 2012, **6**, 6122.
14 R. Dreyfus, J. Baudry, M. L. Roper, M. Fermigier, H. A. Stone and J. Bibette, *Nature*, 2005, **437**, 862.
15 G. Grosjean, G. Lagubeau, A. Darras, M. Hubert, G. Lumay and N. Vandewalle, *Sci. Rep.*, 2015, **5**, 16035.
16 G. Steinbach, S. Gemming and A. Erbe, *Eur. Phys. J. E: Soft Matter Biol. Phys.*, 2016, **39**, 69.
17 A. Kaiser, A. Snezhko and I. S. Aranson, *Sci. Adv.*, 2017, **3**, e1601469.
18 A. Bricard, J.-B. Caussin, N. Desreumaux, O. Dauchot and D. Bartolo, *Nature*, 2013, **503**, 95.
19 A. Morin, N. Desreumaux, J.-B. Caussin and D. Bartolo, *Nat. Phys.*, 2017, **13**, 63.
20 J. R. Howse, R. A. Jones, A. J. Ryan, T. Gough, R. Vafabakhsh and R. Golestanian, *Phys. Rev. Lett.*, 2007, **99**, 048102.
21 C. Bechinger, R. Di Leonardo, H. Löwen, C. Reichhardt, G. Volpe and G. Volpe, *Rev. Mod. Phys.*, 2016, **88**, 045006.
22 W. Gao, D. Kagan, O. S. Pak, C. Clawson, S. Campuzano, E. Chuluun-Erdene, E. Shipton, E. E. Fullerton, L. Zhang, E. Lauga and J. Wang, *Small*, 2012, **8**, 460.
23 B.-W. Park, J. Zhuang, O. Yasa and M. Sitti, *ACS Nano*, 2017, **11**, 8910.
24 Y. Hong, D. Velegol, N. Chaturvedi and A. Sen, *Phys. Chem. Chem. Phys.*, 2010, **12**, 1423.
25 L. Angelani, A. Costanzo and R. Di Leonardo, *EPL*, 2011, **96**, 68002.
26 A. Pototsky, A. M. Hahn and H. Stark, *Phys. Rev. E: Stat., Nonlinear, Soft Matter Phys.*, 2013, **87**, 042124.
27 C. J. Olson Reichhardt and C. Reichhardt, *Annu. Rev. Condens. Matter Phys.*, 2017, **8**, 51–75.
28 A. Zampetaki, P. Schmelcher, H. Löwen and B. Liebchen, *New J. Phys.*, 2018, **21**, 013023.
29 P. Reimann, *Phys. Rep.*, 2002, **361**, 57.
30 P. Hänggi and F. Marchesoni, *Rev. Mod. Phys.*, 2009, **81**, 387.
31 A. K. Mukhopadhyay, B. Liebchen and P. Schmelcher, *Phys. Rev. Lett.*, 2018, **120**, 218002.
32 C. Lozano, B. ten Hagen, H. Löwen and C. Bechinger, *Nat. Commun.*, 2016, **7**, 12828.
33 J. Stenhammar, R. Wittkowski, D. Marenduzzo and M. E. Cates, *Sci. Adv.*, 2016, **2**, e1501850.
34 M. P. Magiera and L. Brendel, *Phys. Rev. E: Stat., Nonlinear, Soft Matter Phys.*, 2015, **92**, 012304.
35 J. Grauer, H. Löwen and L. M. Janssen, *Phys. Rev. E*, 2018, **97**, 022608.
36 A. Geiseler, P. Hänggi, F. Marchesoni, C. Mulhern and S. Savel'ev, *Phys. Rev. E: Stat., Nonlinear, Soft Matter Phys.*, 2016, **94**, 012613.
37 A. Geiseler, P. Hänggi and F. Marchesoni, *Entropy*, 2017, **19**, 97.
38 A. Geiseler, P. Hänggi and F. Marchesoni, *Sci. Rep.*, 2017, **7**, 41884.
39 N. Koumakis, A. T. Brown, J. Arlt, S. E. Griffiths, V. A. Martinez and W. C. K. Poon, 2018, arXiv preprint arXiv: 1811.09133.
40 J. Arlt, V. A. Martinez, A. Dawson, T. Pilizota and W. C. K. Poon, *Nat. Commun.*, 2018, **9**, 768.
41 G. Frangipane, D. Dell'Arciprete, S. Petracchini, C. Maggi, F. Saglimbeni, S. Bianchi, G. Vizsnyiczai, M. L. Bernardini and R. Di Leonardo, *eLife*, 2018, **7**, e36608.
42 J. Arlt, V. A. Martinez, A. Dawson, T. Pilizota and W. C. K. Poon, *Nat. Commun.*, 2019, **10**, 2321.
43 T. Bickel, G. Zecua and A. Würger, *Phys. Rev. E: Stat., Nonlinear, Soft Matter Phys.*, 2014, **89**, 050303.
44 P. Reimann, *Phys. Rep.*, 1997, **290**, 149.
45 Following eqn (3), the orientations of particles in the steep *b*-segments change by a factor a/b faster than in the *a*-segments. Since there are b/a times less particles in the *b*-segments, the overall change in alignment for particles of any given initial orientation in the *b*- and in the *a*-segment is the same. More precisely, consider a representative initial ensemble with

uniformly distributed positions and orientations, *i.e.* with distribution functions $P(x,\phi,0) = 1/(2\pi L)$ for $x \in [0,L)$ and $P(\phi,0) = \int_0^L \mathrm{d}x P(x,\phi,0) = 1/2\pi$. Then, from the Smoluchowski equation corresponding to eqn (1)–(3), after averaging over space, we obtain $P(\phi,\mathrm{d}t) = P(\phi,0)$, where d$t$ represents an infinitesimal time step. Since we are not flashing, this argument can be repeated, yielding $P(\phi,t) = P(\phi,0)$, showing that no net alignment and hence no transport can occur at any time.

46 J. R. Gomez-Solano, S. Samin, C. Lozano, P. Ruedas-Batuecas, R. van Roij and C. Bechinger, *Sci. Rep.*, 2017, 7, 14891.

